INTERNATIONAL JOURNAL FOR NUMERICAL METHODS IN FLUIDS, VOL. 12, 323–342 (1991)

VORTICITY–STREAMFUNCTION FORMULATION OF UNSTEADY INCOMPRESSIBLE FLOW PAST A CYLINDER: SENSITIVITY OF THE COMPUTED FLOW FIELD TO THE LOCATION OF THE OUTFLOW BOUNDARY

M. BEHR, J. LIOU, R. SHIH AND T. E. TEZDUYAR

Department of Aerospace Engineering and Mechanics, and Minnesota Supercomputer Institute, University of Minnesota, Minneapolis, MN 55455, U.S.A.

SUMMARY

The influence of the location of the outflow computational boundary on the unsteady incompressible flow past a circular cylinder at Reynolds number 100 is examined. The vorticity–streamfunction formulation of the Navier–Stokes equations is used in all computations. Two types of outflow boundary conditions are subjected to a series of tests in which the domain length is gradually reduced. The traction-free condition performs well in most cases and allows the outflow boundary to be located as close as 6·5 cylinder diameters from the body. The other boundary condition type is not as forgiving, but has the advantage of being simpler to implement and can still provide reasonably accurate solutions. It is also observed that both condition types can influence the flow field strongly and globally when the boundary is brought closer than 2·5 diameters from the body. In such cases the temporal periodicity of the solution is lost.

KEY WORDS Vorticity–streamfunction formulation Outflow boundary conditions

1. INTRODUCTION

The choice of the size and shape of the computational domain is an important part of every numerical simulation. In some cases it is possible to place the domain boundaries exactly as dictated by the problem being modelled; but frequently the physical domain is too large (perhaps infinitely large) to be represented fully, and truncation of the model size is necessary to make the numerical task manageable. One can simply hope that the computational boundaries so introduced do not degrade the quality of the results in the region of interest. In incompressible flow problems the outflow boundary is usually only an approximation to the flow field extending farther downstream. This boundary can play an important role in determining the solution. Therefore care must be taken to ensure that the numerical boundary conditions employed, as well as the point of their application, result in faithful representation of the flow field despite the truncation of the domain.

The research which led to the material presented here was motivated by a series of discussions with P. M. Gresho[1] and an upcoming outflow boundary condition (OBC) symposium (Stanford University, Stanford, CA, July 1991). We attempt to provide a few guidelines for the placement of the outflow boundary and the choice of OBC type. For this purpose, for flow past a circular cylinder, we study the behaviour of significant flow quantities, namely the drag, lift and Strouhal

0271–2091/91/040323–20$10.00

Received 9 May 1990

number, as the downstream part of the mesh is truncated. This procedure closely follows similar experiments performed within the framework of the velocity–pressure formulation.[2] We also examine two different types of OBC which arise in the context of the vorticity–streamfunction formulation of the Navier–Stokes equations in two dimensions. The first type of OBC is the *homogeneous* form of the *natural* boundary conditions associated with the vorticity transport equation and the Poisson equation for the streamfunction; we will refer to this as the HN-type OBC. This OBC implies vanishing normal derivatives for the vorticity and streamfunction at the outflow boundary. While the assumption of zero normal derivative for the vorticity is quite reasonable for advection-dominated flows, similar treatment of the streamfunction results in zero tangential velocity at the boundary. This restriction of course influences the flow field upstream of the boundary, and such undesirable influence has to be weighed against the simplicity of the HN-type OBC. The second type of OBC is the vorticity–streamfunction equivalent of the *traction-free* condition commonly seen in velocity–pressure formulations (see e.g. Reference 3). This OBC assumes zero normal and shear stresses; we will refer to it as the TF-type OBC.

The spatial discretization of the governing equations is based on the streamline-upwind/Petrov–Galerkin (SUPG) modification of the finite element formulation employing bilinear shape functions for both the vorticity and streamfunction. A central-difference-type temporal discretization is used and the fully coupled equations involving all the unknowns are solved simultaneously at each time level.

2. FORMULATION OF THE PROBLEM

Consider an incompressible fluid occupying an open bounded region $\Omega \in \mathbb{R}^2$. The boundary of Ω is denoted by Γ, and this boundary consists of an external boundary Γ_0 and q internal boundaries denoted by Γ_k, $k=1, 2, \ldots, q$, such that

$$\Gamma = \Gamma_0 \cup \Gamma_1 \cup \ldots \cup \Gamma_q. \tag{1}$$

The fluid velocity vector is denoted by $\mathbf{u}(\mathbf{x}, t)$, where $\mathbf{x} \in \Omega$ and $t \in [0, T]$, a given time interval. The vorticity $\omega(\mathbf{x}, t)$ and streamfunction $\psi(\mathbf{x}, t)$ are defined by

$$\omega = \frac{\partial u_2}{\partial x_1} - \frac{\partial u_1}{\partial x_2}, \tag{2}$$

$$\mathbf{u} = \left\{ \frac{\partial \psi}{\partial x_2}, -\frac{\partial \psi}{\partial x_1} \right\}. \tag{3}$$

The vorticity–streamfunction formulation of the two-dimensional incompressible Navier–Stokes equations is given as

$$\frac{\partial \omega}{\partial t} + \mathbf{u} \cdot \nabla \omega - \nu \nabla^2 \omega = 0 \quad \text{on } \Omega \times (0, T), \tag{4}$$

$$\nabla^2 \psi + \omega = 0 \quad \text{on } \Omega \times (0, T), \tag{5}$$

with initial condition

$$\omega(\mathbf{x}, 0) = \omega_0(\mathbf{x}), \quad \mathbf{x} \in \Omega. \tag{6}$$

Here ν is the kinematic viscosity of the fluid. The problem statement is completed by imposing suitable boundary conditions on the vorticity and streamfunction. Let $\Gamma_{0d} \subset \Gamma_0$ be the downstream

(outflow) boundary, treated separately to facilitate the choice of two alternative types of OBC. The HN-type OBC is the homogeneous natural boundary condition associated with (4) and (5) and can be expressed as follows:

$$\frac{\partial \psi}{\partial n}=0 \qquad \text{on } \Gamma_{0d}\times(0, T), \tag{7}$$

$$\frac{\partial \omega}{\partial n}=0 \qquad \text{on } \Gamma_{0d}\times(0, T). \tag{8}$$

The TF-type OBC, which was derived in Reference 4, is equivalent to the homogeneous natural boundary conditions for the momentum equation in the velocity–pressure formulation with the stress divergence form. These conditions imply zero normal and tangential stresses at the boundary; they can be respectively written as

$$\frac{\partial u_\tau}{\partial t}+u_\tau\frac{\partial u_\tau}{\partial \tau}-2\nu\frac{\partial^2 u_\tau}{\partial \tau^2}=-\frac{1}{2}\frac{\partial(\partial\psi/\partial\tau)^2}{\partial\tau}-\frac{\partial\psi}{\partial\tau}\omega-\nu\frac{\partial\omega}{\partial n} \quad \text{on } \Gamma_{0d}\times(0, T), \tag{9}$$

$$2\frac{\partial^2\psi}{\partial\tau^2}=-\omega \quad \text{on } \Gamma_{0d}\times(0, T), \tag{10}$$

where n and τ represent the normal and tangential coordinates along Γ_{0d}, and u_τ is the tangential component of the velocity vector. This type of OBC is commonly known as the traction-free condition. Equations (9) and (10) can be used to determine, respectively, u_τ and ψ on Γ_{0d}. At this Reynolds number (i.e., 100) it is reasonable to assume that the flow is nearly inviscid at the downstream boundary; therefore we discard the outflow boundary condition given by (10) and replace it with the zero-normal-derivative condition for the vorticity. Equation (9) is then discretized using the finite element approximation in space and the trapezoidal rule in time to form a secondary system of equations. This system is solved at every time step in a block iteration fashion along with the equation system resulting from (4) and (5) until a predetermined convergence condition is met. The full description of the boundary conditions on the parts of Γ other than Γ_{0d} is omitted here and the reader is referred to Reference 5 for details.

To compute the drag and lift on the cylinder, it is necessary to recover the pressure distribution on the cylinder surface from the known vorticity and streamfunction fields. An arbitrary pressure value p_1 is assumed at a reference point on the obstacle surface, and the following line integral is used to calculate the pressure p_2 at other surface points:

$$p_2-p_1=-\rho\int_1^2 \nu\frac{\partial\omega}{\partial n}\,d\tau. \tag{11}$$

The normal and tangential components of the stress on a solid surface,

$$\sigma_n=-p, \tag{12}$$

$$\sigma_\tau=-\rho\nu\omega, \tag{13}$$

can then be numerically integrated along the surface to give the drag and lift on the obstacle.

The governing equations (4) and (5) are discretized by using bilinear shape functions for both the vorticity and streamfunction. The internal boundary gives rise to an additional variational equation for the unknown value of the streamfunction there. The full description of the discretization procedure can be found in Reference 5. If the TF-type OBC is used, equation (9) leads to the additional equations needed to determine the value of u_τ on Γ_{0d}.

3. NUMERICAL RESULTS

As the test problem for which the influence of the outflow boundary condition is to be investigated, we choose a well-known, yet non-trivial two-dimensional case. Wake formation behind a circular cylinder has attracted the attention of many researchers in the past and thus provides us with a large pool of experimental and numerical results. At the same time the complex Karman vortex street extending downstream of the cylinder for sufficiently large Reynolds numbers makes the detection of the boundary-induced changes in the solution simple.

In all results presented here the Reynolds number based on the cylinder diameter of 2·0 and the uniform free-stream velocity of 0·125 is 100. All linear dimensions are normalized by the cylinder diameter. The computational domain extends 8 units upstream and in both cross-flow directions, as measured from the cylinder centre. The location of the downstream boundary is different for each mesh used, as shown in Table I. In further references to various mesh configurations we will adopt the following naming convention: the shortest mesh is denoted as mesh 000; the longest mesh, which is 22·5 units longer than mesh 000, will be referred to as mesh 225. In all other cases the names are assigned in a similar fashion. The longest domain is drawn to scale in Figure 1.

The numbers of nodes and quadrilateral elements for each mesh are also given in Table I. Our previous experience with the cylinder problem indicates that any additional mesh refinement only increases the computational burden, without significant improvement in the quality of the solution. Mesh 000 forms the basis for all other meshes, which are constructed by simply adding a number of uniform elements downstream.

The upper and lower boundaries are assumed to be flow symmetry lines (in the Appendix we also discuss the tow tank boundary conditions in the context of the velocity–pressure formulation). A uniform velocity is assumed at the upstream boundary. Both HN- and TF-type OBCs are tested. For both types of OBC the computations were initially performed for mesh 225, starting with $\omega_0 \equiv 0$ in the entire domain, and were continued until temporally periodic vortex

Table I. The mesh parameters

Mesh	Distance B (see Figure 1)	Number of nodes	Number of elements
000	2·5	2724	2608
040	6·5	3084	2960
080	10·5	3444	3312
120	14·5	3804	3664
160	18·5	4164	4016
200	22·5	4524	4368
225	25·0	4749	4588

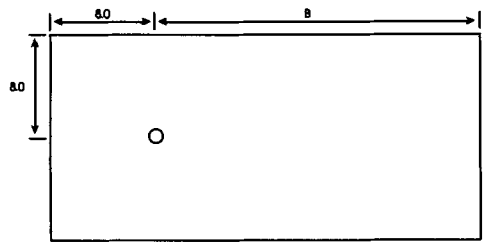

Figure 1. The computational domain

shedding was achieved. The periodic solution obtained with mesh 225 was then used as the initial condition for mesh 200. By always initializing the solution for a given mesh with an already periodic solution from the closest longer mesh, we were able to speed up the convergence to the temporally periodic solution. The time step chosen for all computations is 0·125, providing us with a good resolution of the vortex-shedding period, lasting about 730 time steps.

The time histories of the drag and lift coefficients for various meshes along with the corresponding Strouhal number (defined as $St=fd/U$, where f is the frequency of the vortex shedding, U is the free-stream velocity, and d is the cylinder diameter) values are shown in Figures 2–5. The mean and amplitude of the drag, the amplitude of the lift and the Strouhal number are

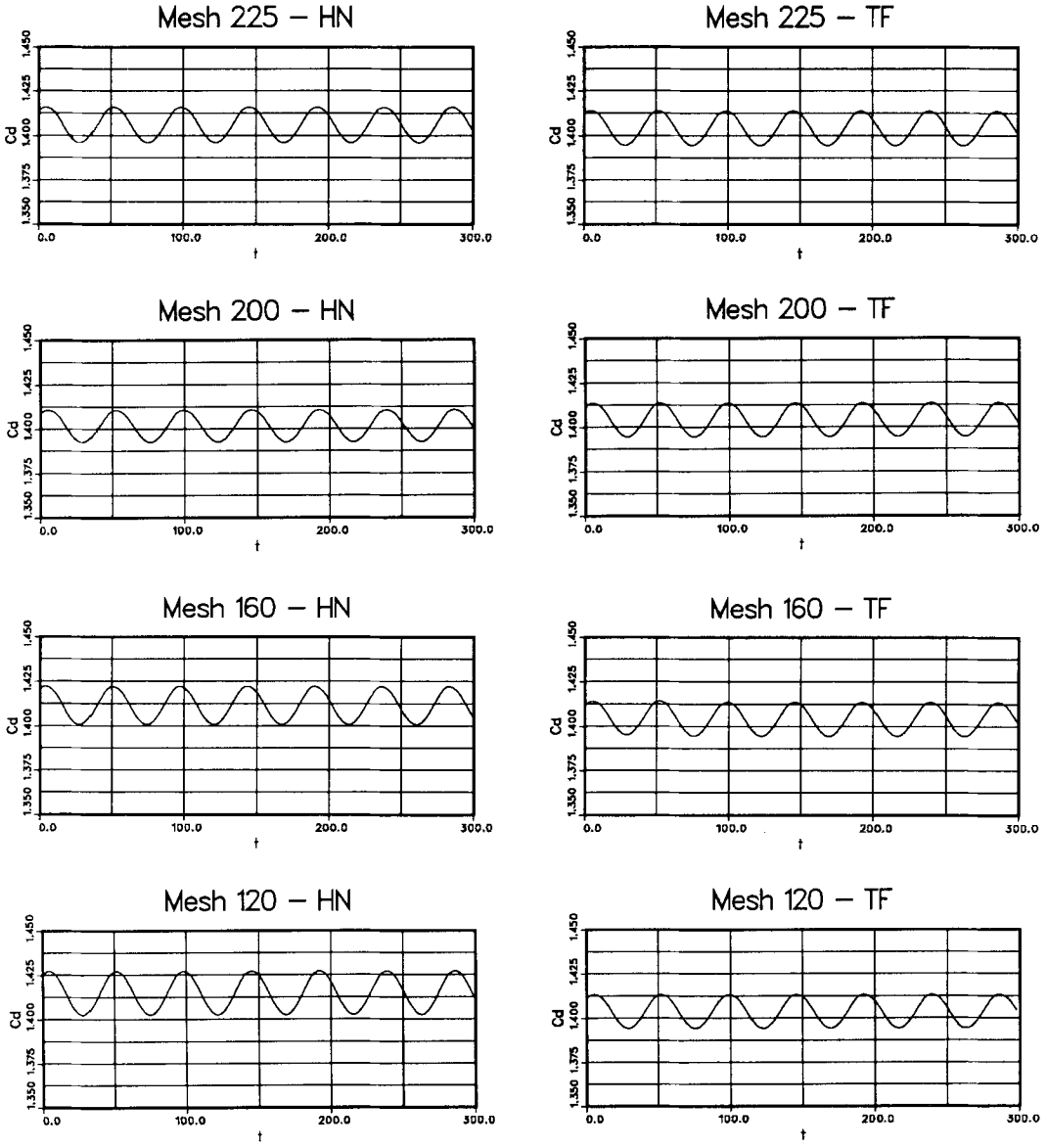

Figure 2. Time history of the drag coefficient for the longer meshes

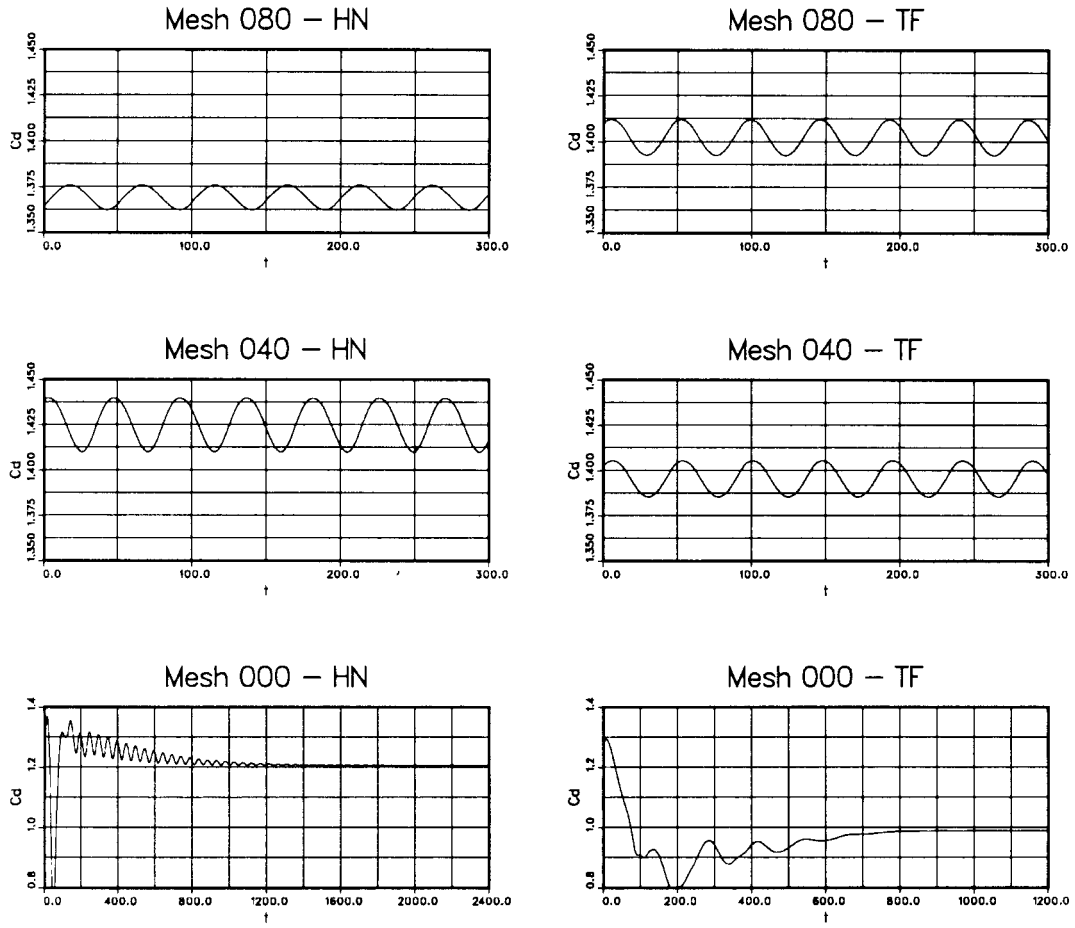

Figure 3. Time history of the drag coefficient for the shorter meshes (note the change of scale for mesh 000)

plotted against the mesh length in Figures 6–8. The periodic flow patterns corresponding to the crest value of the lift coefficient are presented in Figures 9–15. In the plots of the drag and lift coefficients, $t=0$ is assigned to a crest value of the lift coefficient.

For the TF-type OBC, for all meshes except mesh 000, we obtain the same values for the drag and lift coefficients and the Strouhal number. For mesh 000, because the downstream boundary is placed too close to the cylinder, the stability of the periodic flow field is disturbed and instead a steady solution is obtained. All in all, our version of the traction-free outflow boundary condition exerts very little influence on the flow field, allowing the relevant boundary to be brought as close as 6·5 diameters to the body, with no more than 0·5% change in the lift and drag coefficients and with no visible changes in the flow patterns.

The situation is different when the HN-type OBC is used. Even for the longer meshes we observe slight variations in the drag coefficient. As the mesh is truncated, the average drag coefficient strays significantly from the value of 1·405 obtained with mesh 225. For mesh 080 this difference is -3%; for mesh 040 it amounts to 2%. For the amplitude of the lift coefficient and the Strouhal number we also see large changes for meshes 080 and 040 but little or no variation for longer

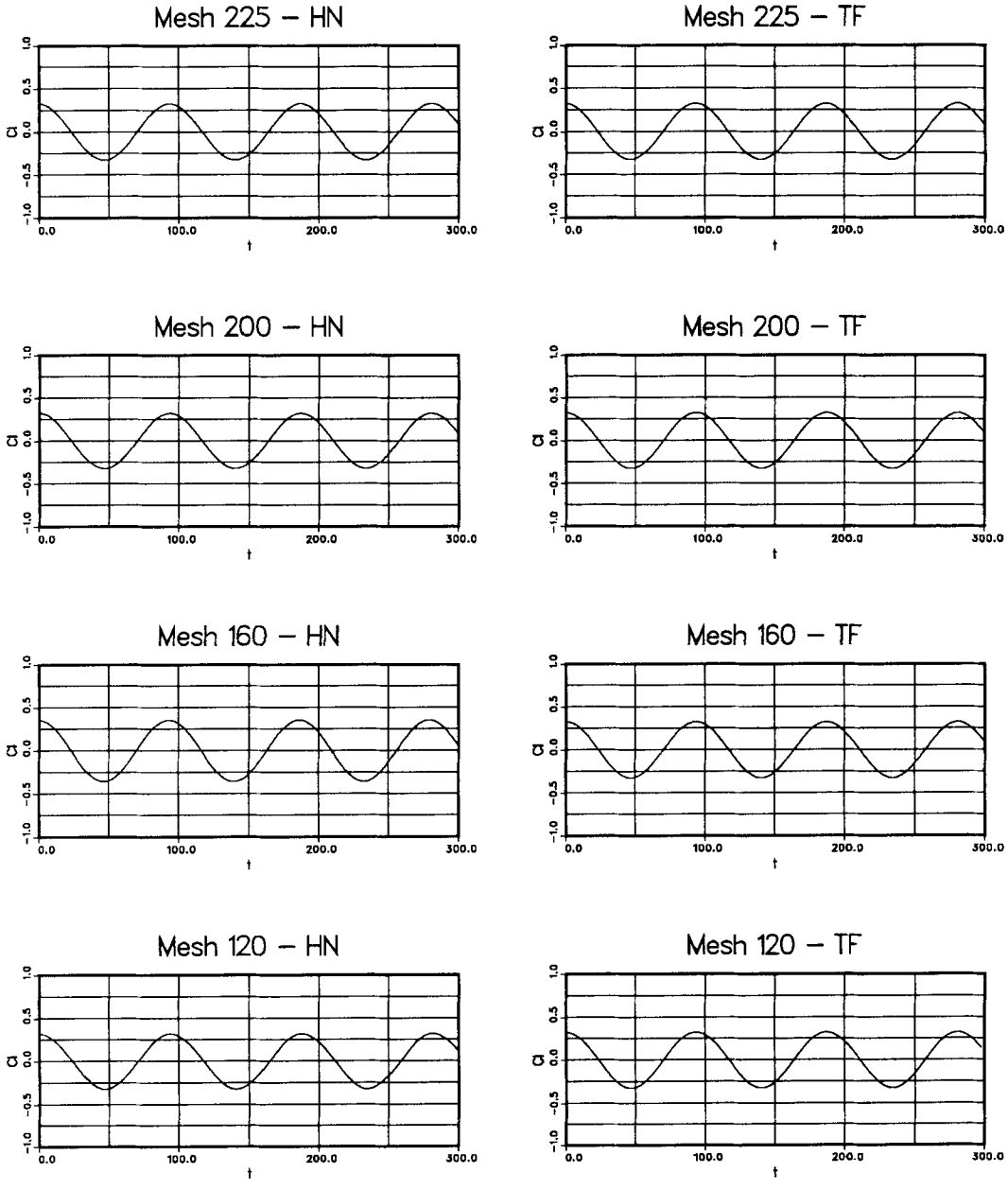

Figure 4. Time history of the lift coefficient for the longer meshes

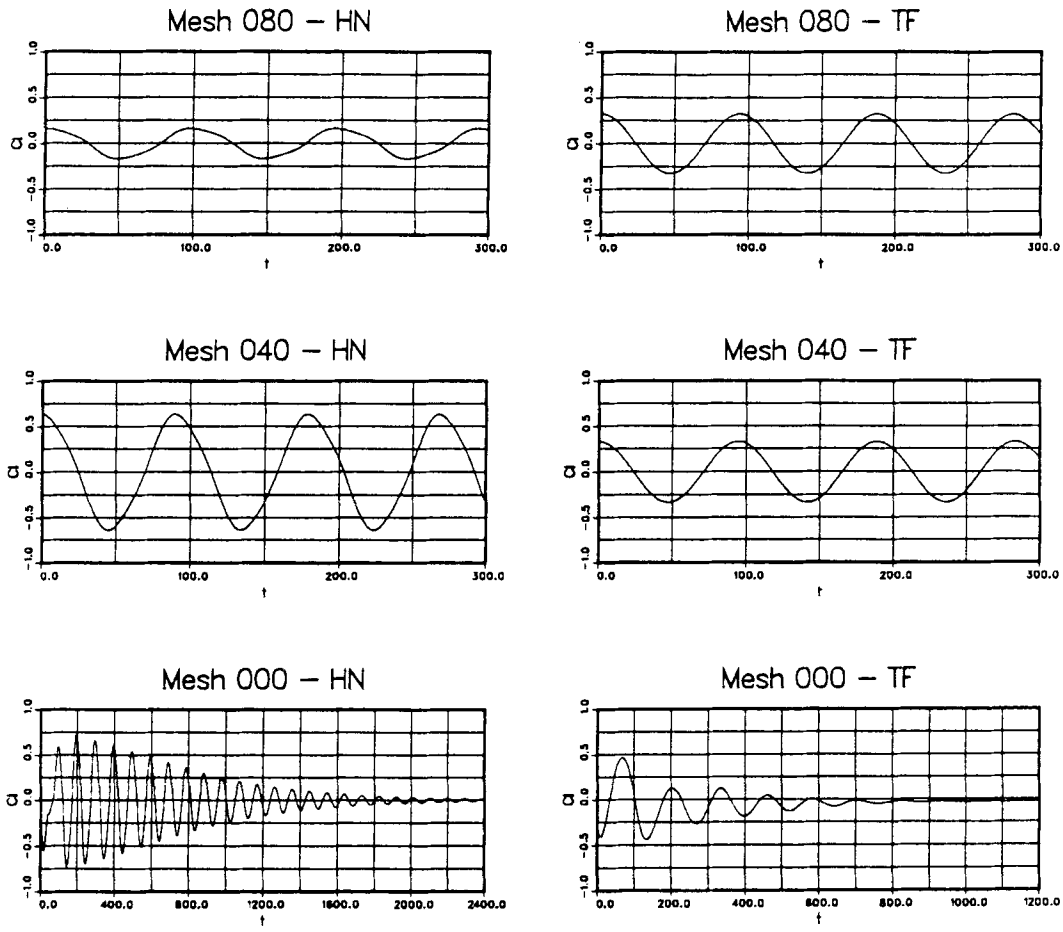

Figure 5. Time history of the lift coefficient for the shorter meshes

domains. Finally, for mesh 000 the solution again loses its temporal periodicity and tends to a steady state solution different from the one obtained by using the TF-type OBC (see Figure 15). For all meshes there are observable alterations in the downstream streamline patterns, since the streamlines must be perpendicular to the boundary to satisfy (7). The numerical code employing the HN-type OBC was observed to be about 10% faster than the code involving the TF-type OBC.

It should be noted that the TF-type OBC used in conjunction with mesh 000 admits not one but at least two distinct steady state solutions. As seen in Figure 15, the time-dependent algorithm produces an asymmetric steady flow pattern if the temporally periodic solution from mesh 040 is used as the initial condition. However, when that initial condition is replaced by the symmetric steady flow (similar to the final solution for the HN-type OBC) obtained with a steady state algorithm, the flow remains symmetric and steady. In fact both the symmetric and asymmetric solutions satisfy both the time-dependent and steady state equations.

The results described here for the TF-type OBC agree well with a similar study reported in Reference 2, where the velocity–pressure variables were used in place of the vorticity and streamfunction.

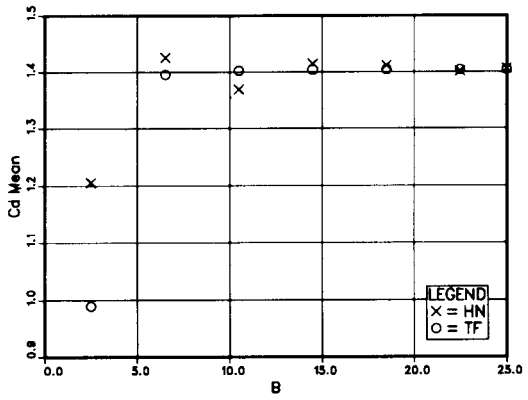

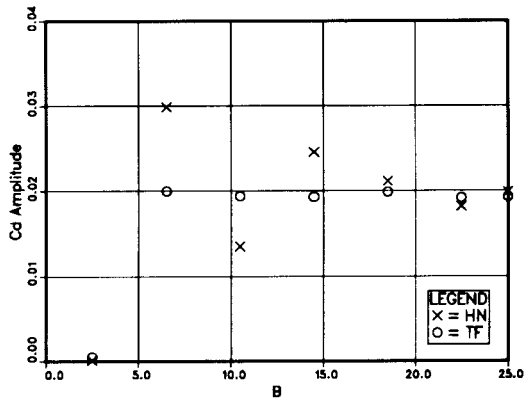

Figure 6. Variation of the drag coefficient with the mesh length

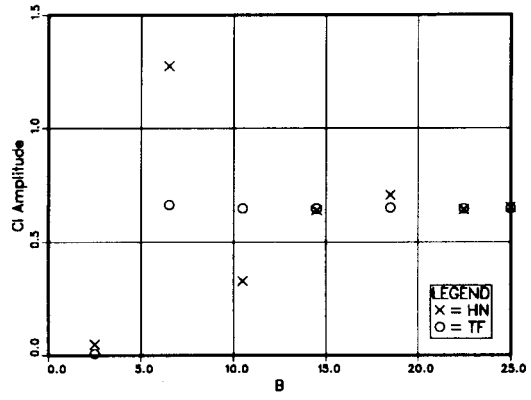

Figure 7. Variation of the lift coefficient with the mesh length

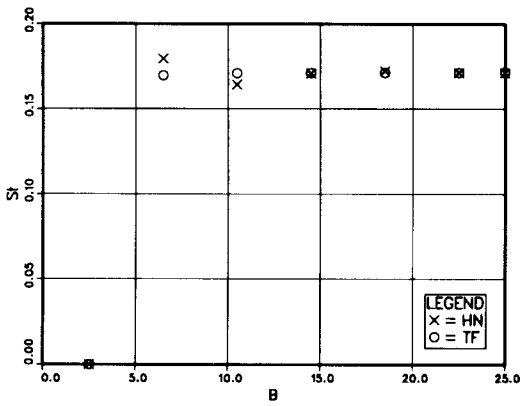

Figure 8. Variation of the Strouhal number with the mesh length

4. CONCLUSIONS

We presented a set of results for the flow past a circular cylinder at Reynolds number 100 to check the proper placement of the outflow boundary in the presence of wakes in the flow field. We also compared the two types of outflow boundary conditions available in the vorticity–streamfunction formulation of the Navier–Stokes equations. By using a number of meshes with differing lengths, we computed the drag and lift coefficients obtained with each mesh. We also measured the frequency of the vortex shedding. For each mesh the computations were initialized with the temporally periodic solution obtained with the next longer mesh, if available, and were continued until the fully periodic solution was reached or until the periodicity was lost in the case of the shortest mesh.

On the basis of these numerical results we conclude that when the TF-type OBC is used we may position the outflow boundary as close as 6·5 cylinder diameters from the cylinder centre without any significant variations in the observed quantities or the general appearance of the near-field solutions. Moreover, when that distance is reduced to 2·5 diameters, the temporal periodicity of the solution is lost and the flow becomes steady. When the HN-type OBC is employed, reliable values for the drag and lift coefficients and the Strouhal number can be obtained with the distance between the boundary and the cylinder centre as low as 14·5 diameters. Similar to the previous case, when the HN-type OBC is imposed at 2·5 diameters from the cylinder centre, the solution becomes unacceptably altered and loses its periodic nature. For both types of OBCs the critical distance between the outflow boundary and the cylinder centre, for which the solution becomes steady falls between 6·5 and 2·5 diameters.

ACKNOWLEDGEMENTS

This research was sponsored by NASA—Johnson Space Center under contract NAS-9-17892 and by NSF under grant MSM-8796352.

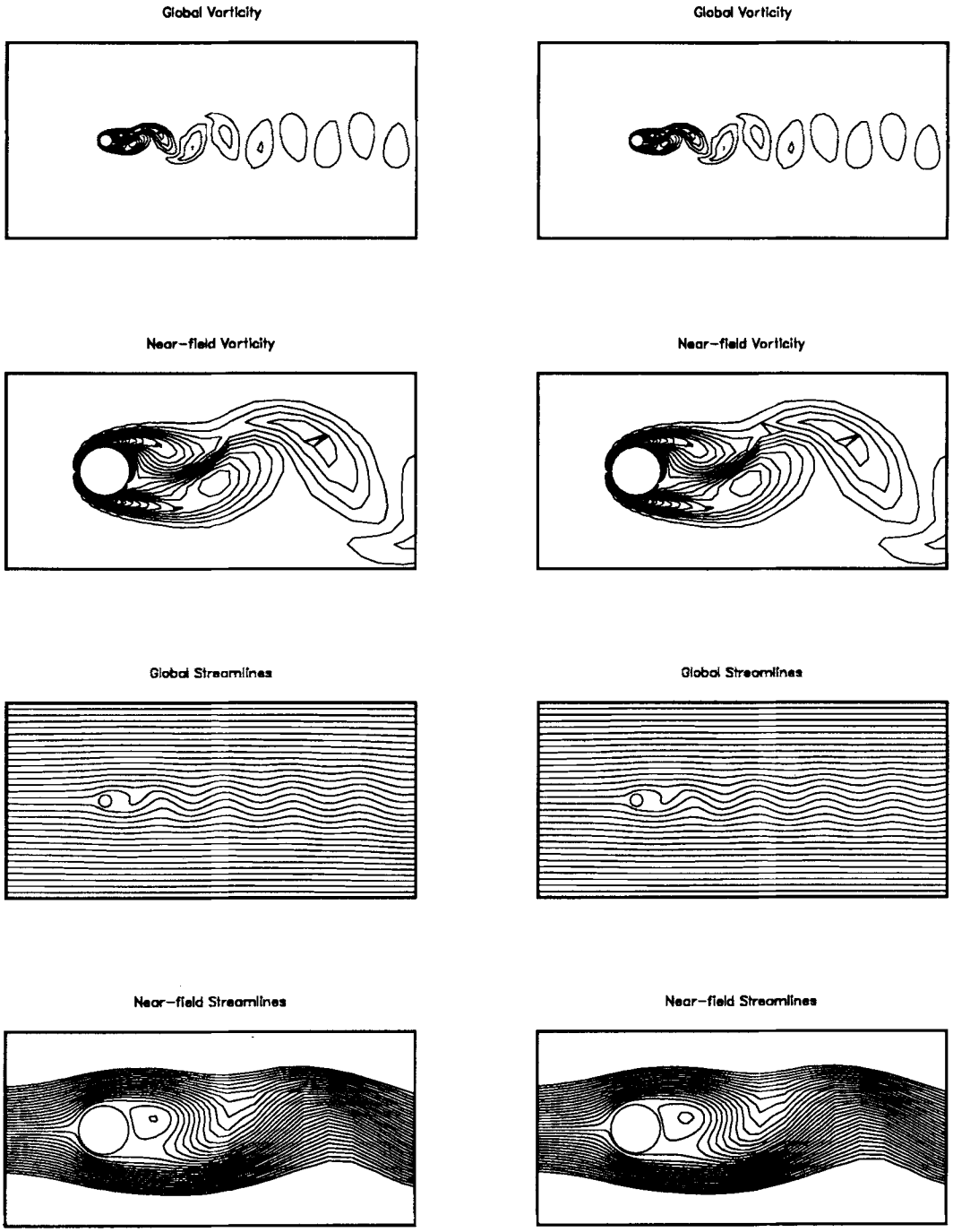

Figure 9. Mesh 225: periodic solutions (corresponding to the crest value of the lift coefficient) obtained with HN (left) and TF (right)

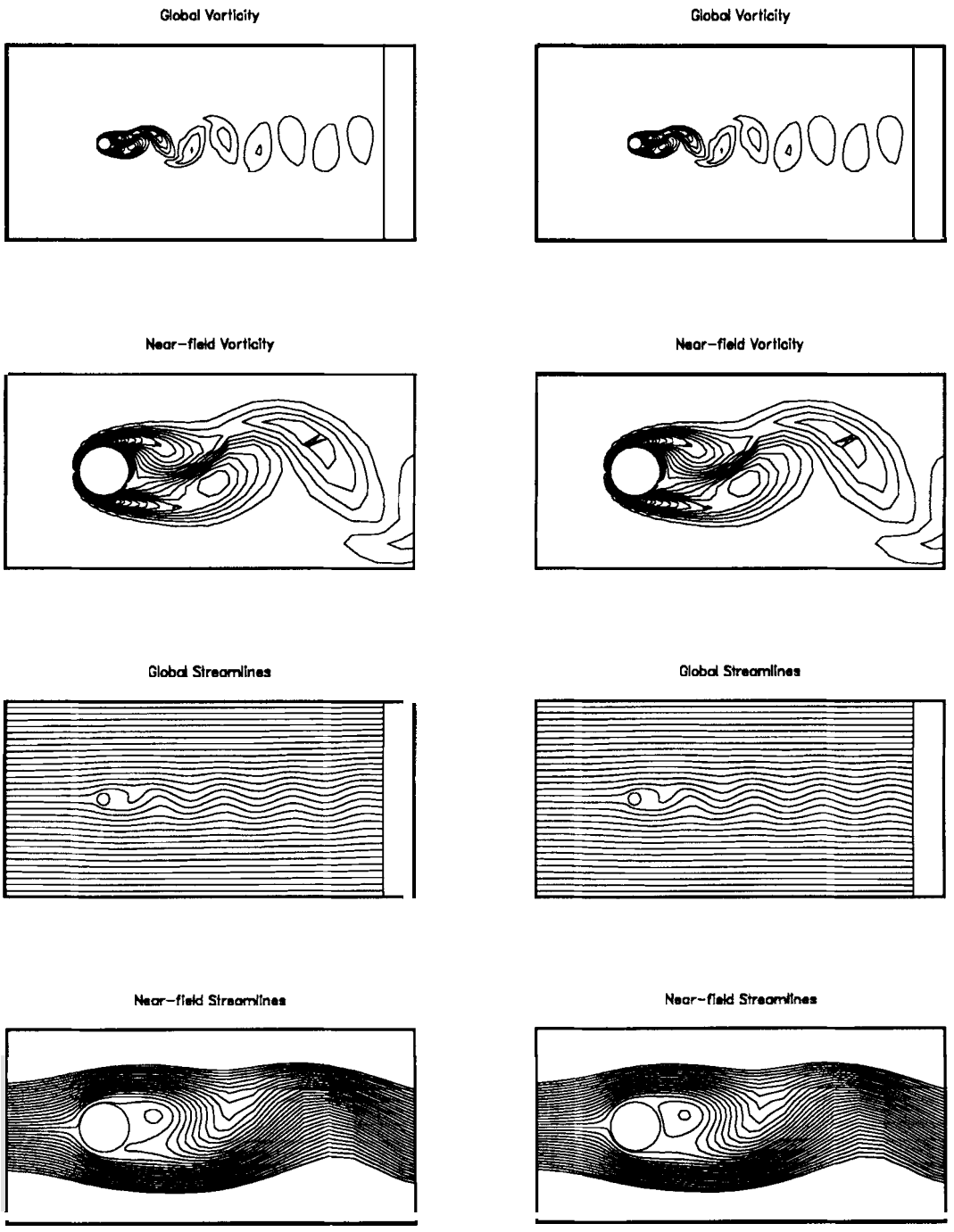

Figure 10. Mesh 200: periodic solutions (corresponding to the crest value of the lift coefficient) obtained with HN (left) and TF (right)

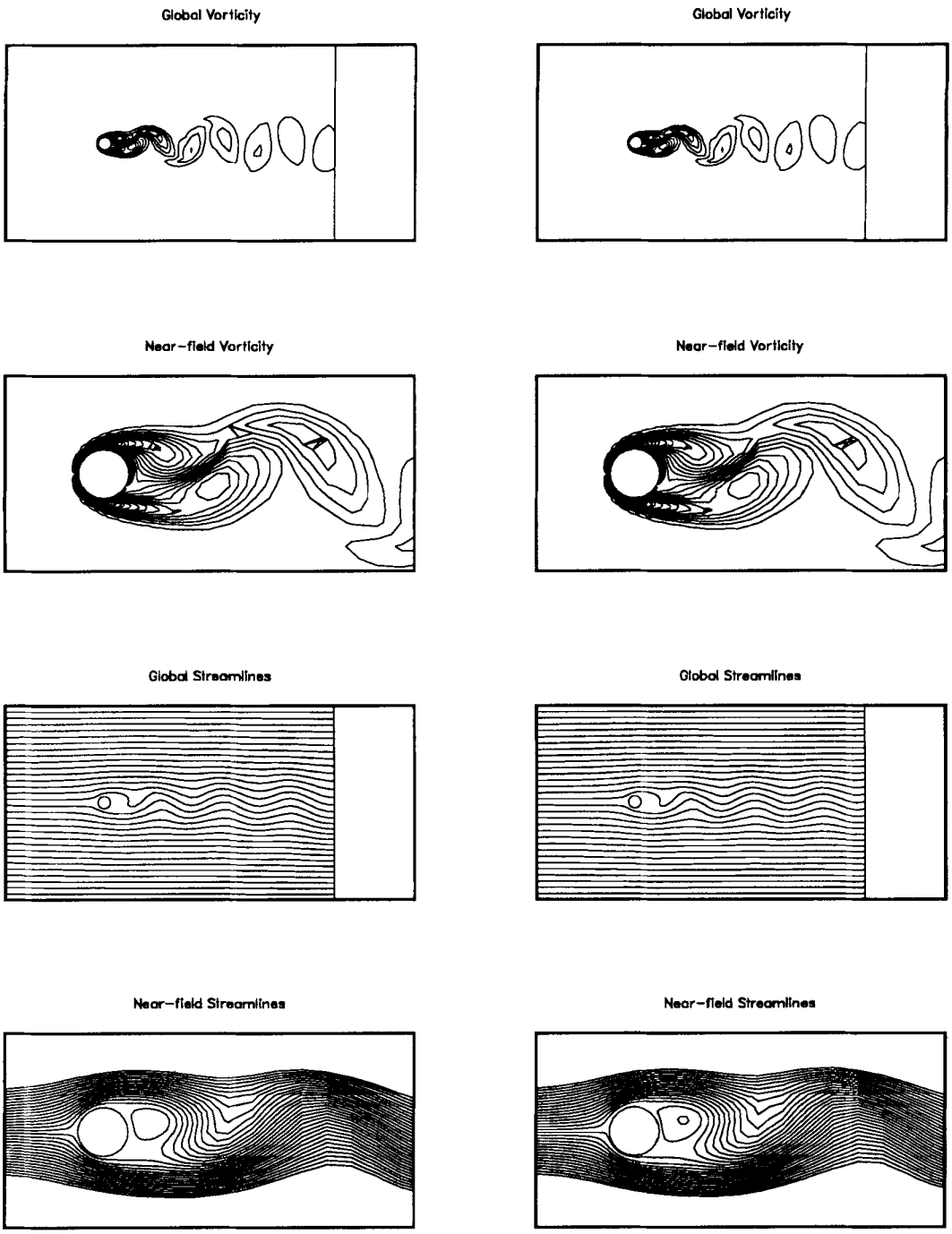

Figure 11. Mesh 160: periodic solutions (corresponding to the crest value of the lift coefficient) obtained with HN (left) and TF (right)

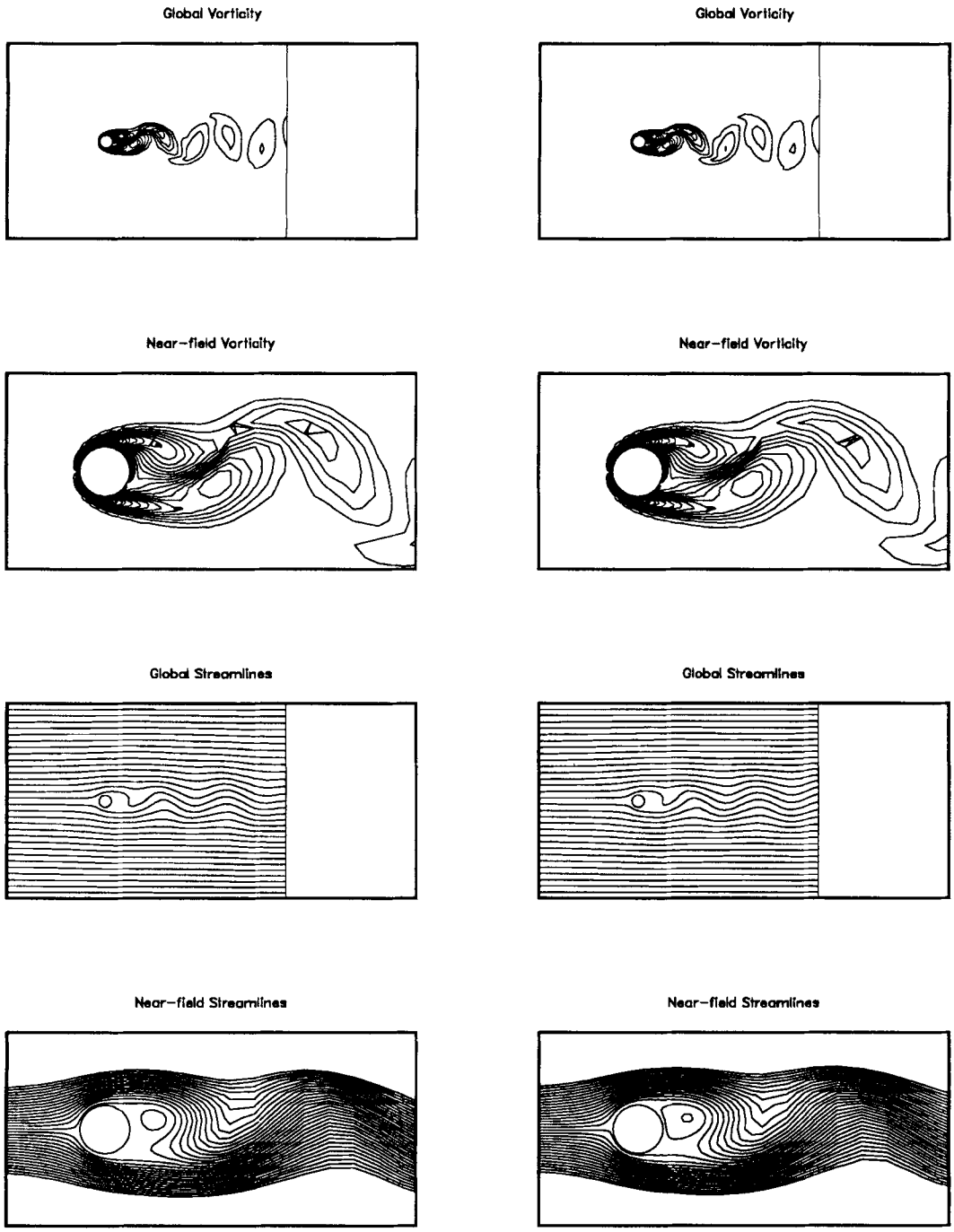

Figure 12. Mesh 120: periodic solutions (corresponding to the crest value of the lift coefficient) obtained with HN (left) and TF (right)

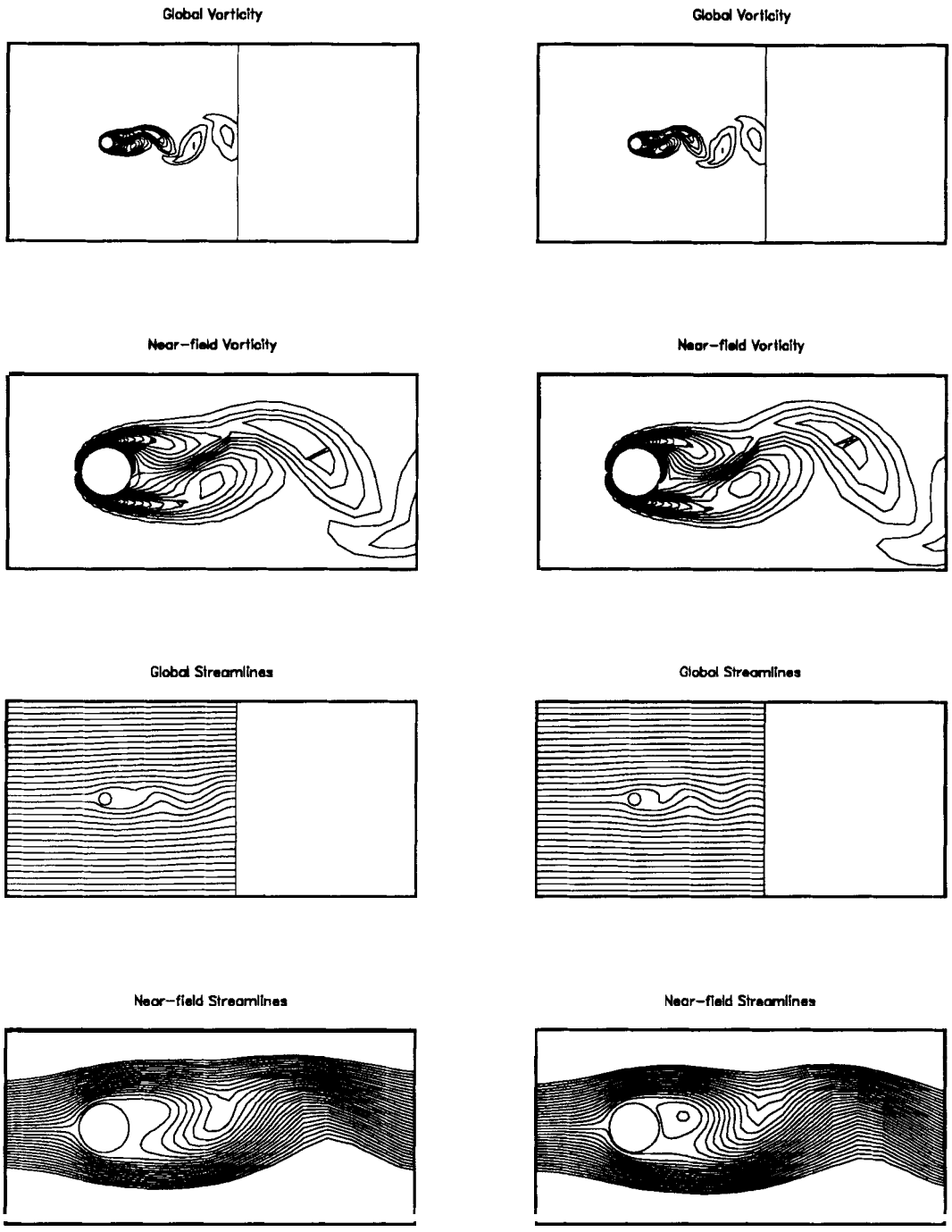

Figure 13. Mesh 080: periodic solutions (corresponding to the crest value of the lift coefficient) obtained with HN (left) and TF (right)

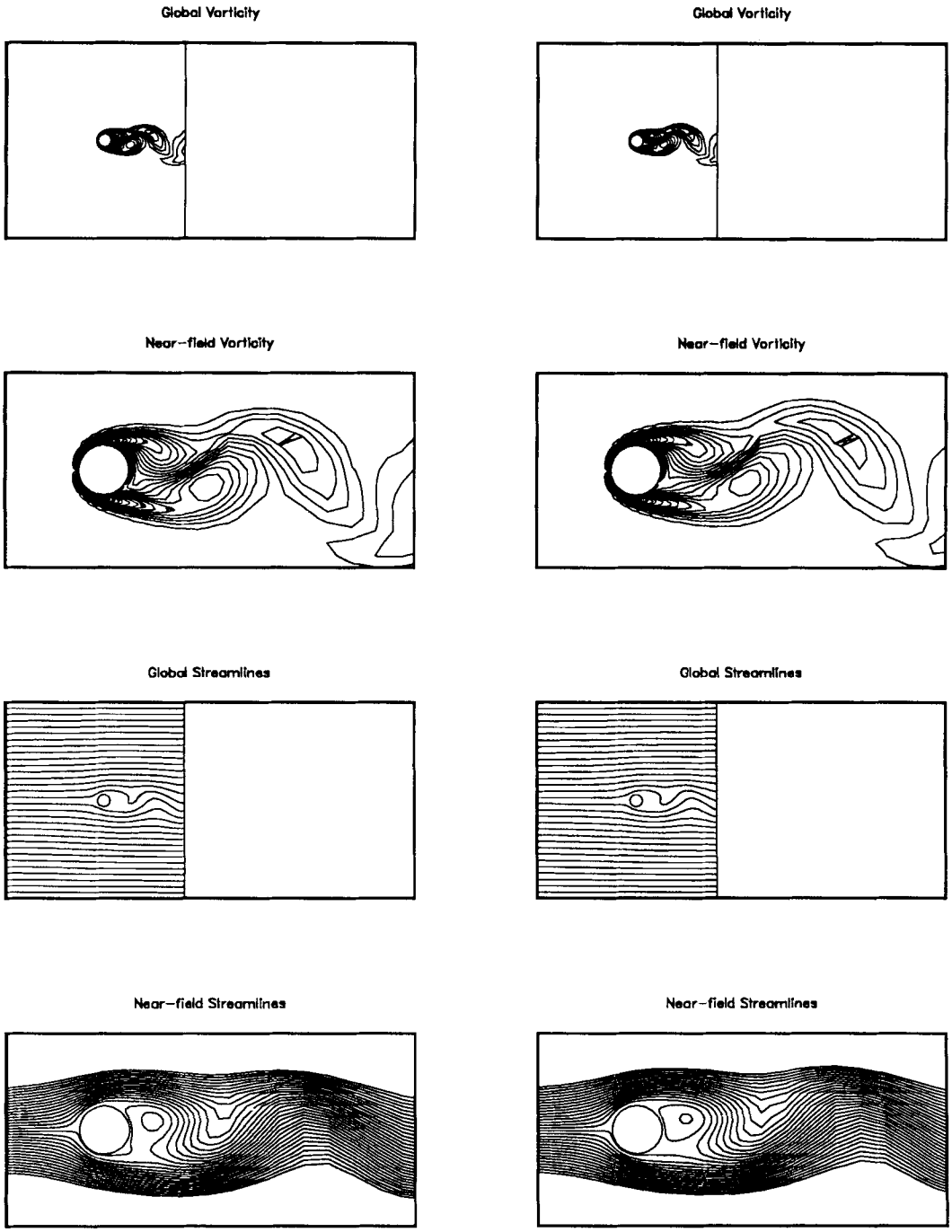

Figure 14. Mesh 040: periodic solutions (corresponding to the crest value of the lift coefficient) obtained with HN (left) and TF (right)

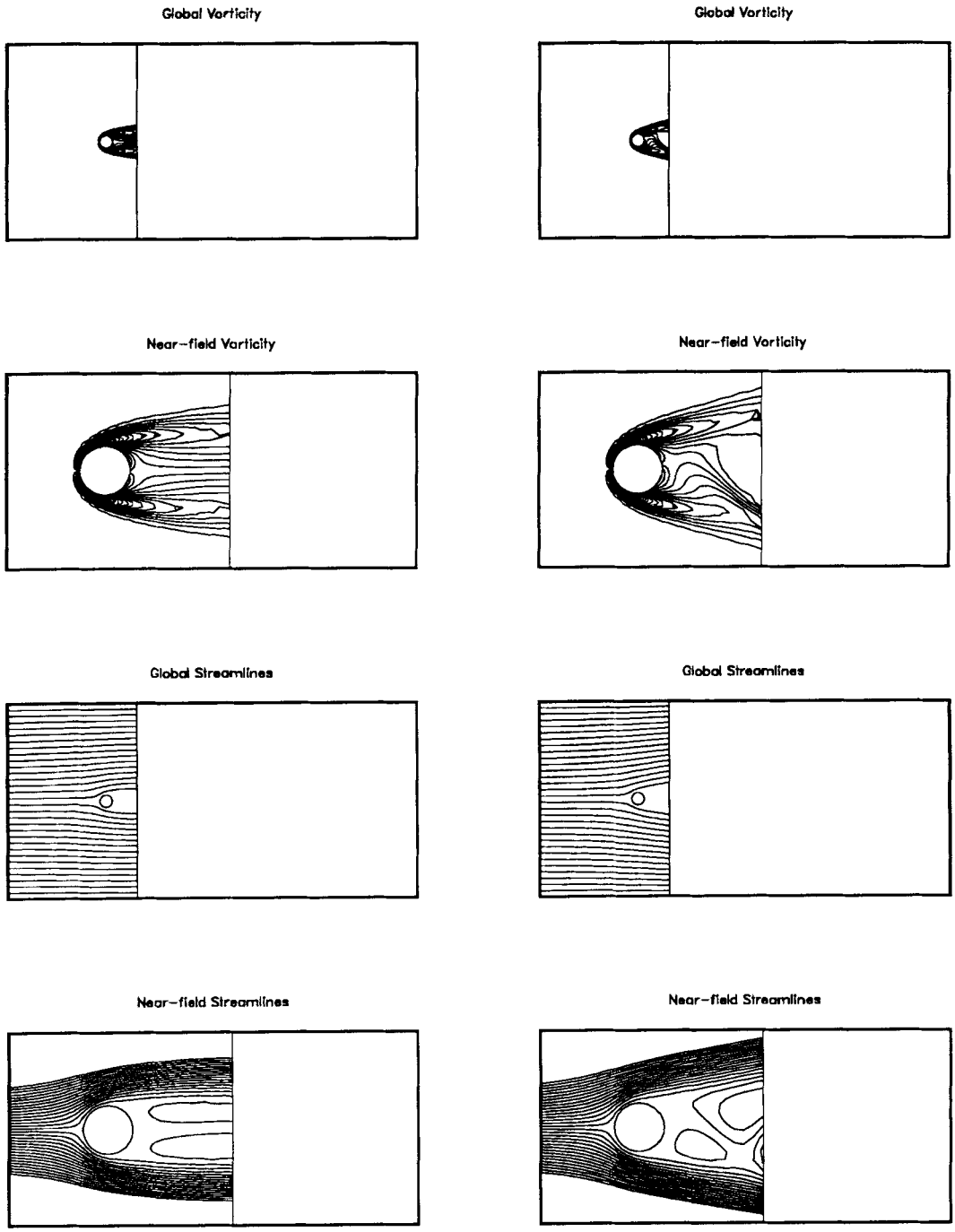

Figure 15. Mesh 000: solutions obtained with HN (left) and TF (right)

APPENDIX: SELECTED NUMERICAL EXPERIMENTS WITH THE VELOCITY–PRESSURE FORMULATION

In this appendix we repeat our experiments for certain cases, which were not described in Reference 2, related to the velocity–pressure formulation. These cases, which were investigated in Reference 6, involve configurations which were agreed on as designated test geometries at the international (and unpublished) mini-symposium on outflow boundary conditions held at the University of Wales, Swansea, U.K. in July 1989. One such geometry is the shortest mesh considered in Reference 6; it coincides with our meshes as far as the upstream and the upper and lower boundaries are concerned, but extends 4·0 units downstream from the cylinder centre, and thus falls between mesh 000 and mesh 040. We will refer to it as mesh 015. The second geometry is the longest mesh investigated in Reference 6, with downstream boundary located 25·2 units from the cylinder centre, and therefore is almost the same as our mesh 225. Also in the aforementioned symposium, the so-called tow tank boundary condition was designated as the condition at the upper and lower computational boundaries. The tow tank boundary condition imposes the free-stream velocity, and as such, it differs from the symmetry boundary condition used in our computations. We conducted numerical experiments for meshes 225 and 015 with both types of boundary conditions and found that the tow tank and symmetry conditions lead to almost identical results. In all computations performed within the velocity–pressure formulation we use traction-free outflow boundary conditions. In Figure 16 we present the time history of the drag and lift coefficients for meshes 225 and 015 obtained with both symmetry and tow tank conditions. Table II provides the parameters for the two meshes. Table III shows, for all four cases discussed in this appendix, the mean and amplitude of the drag, the amplitude of the lift and the Strouhal number.

Table II. The mesh parameters

Mesh	Distance B (see Figure 1)	Number of nodes	Number of elements
015	4·0	2859	2740
225	25·0	4749	4588

Table III. Summary of the results for the Appendix

Case	Cd mean	Cd amplitude	Cl amplitude	Strouhal number
Mesh 015: symmetry	1·380	0·033	0·857	0·165
Mesh 015: tow tank	1·383	0·033	0·858	0·166
Mesh 225: symmetry	1·413	0·026	0·808	0·174
Mesh 225: tow tank	1·415	0·026	0·809	0·174

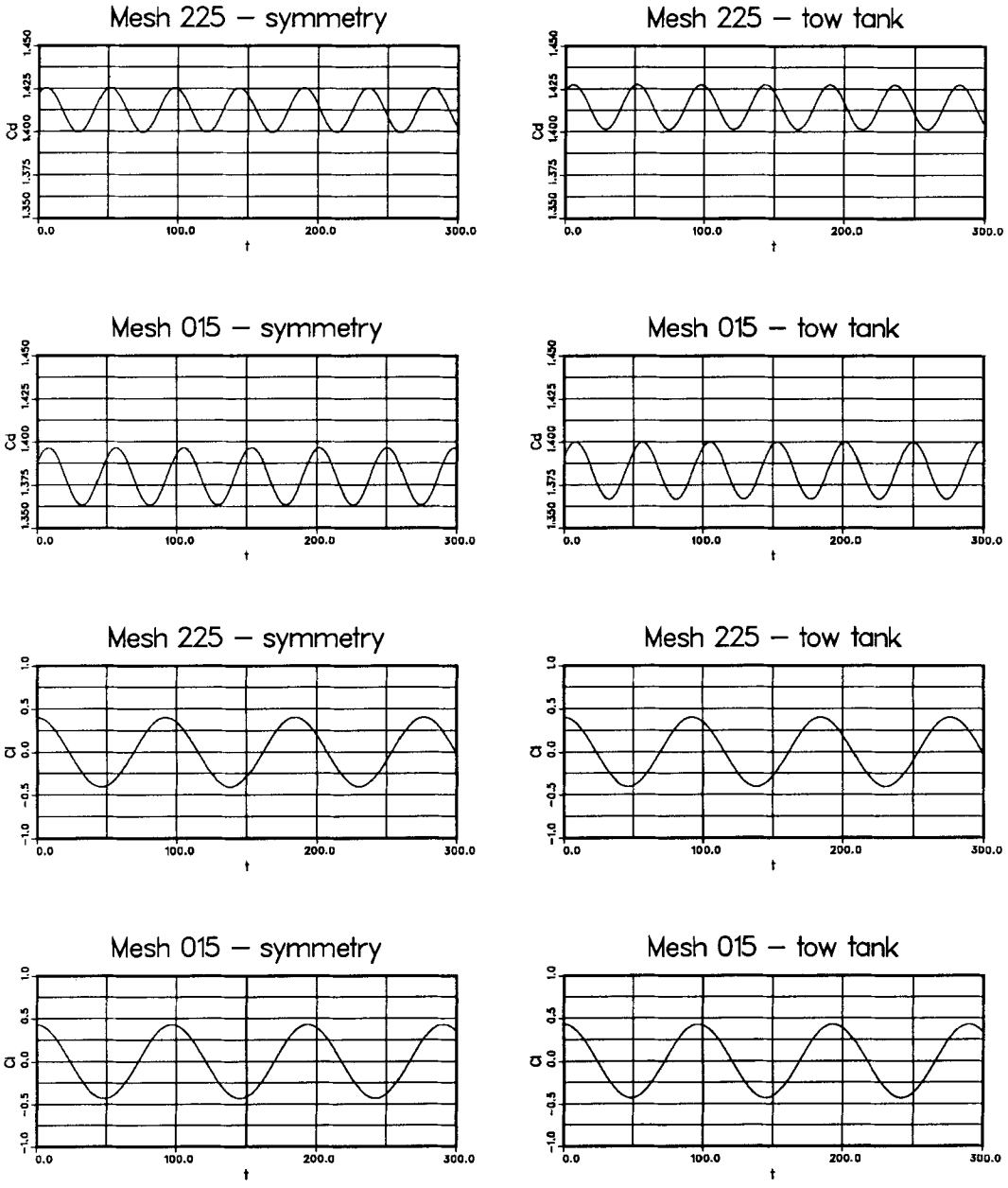

Figure 16. Time history of the drag and lift coefficients for the meshes discussed in the Appendix

REFERENCES

1. P. M. Gresho, Private communications, 1989–1990.
2. R. Shih and T. E. Tezduyar, 'Numerical experiments with the location of the downstream boundary for flow past a cylinder', *University of Minnesota Supercomputer Institute Report UMSI 90/38*, 1990, to appear in *Journal of Engineering Mechanics*.
3. A. N. Brooks and T. J. R. Hughes, 'Streamline-upwind/Petrov–Galerkin formulations for convection dominated flows with particular emphasis on incompressible Navier–Stokes equation', *Comput. Methods Appl. Mech. Eng.*, **32**, 199–259 (1982).
4. T. E. Tezduyar and J. Liou, 'On the downstream boundary conditions for the vorticity–stream function formulation of two-dimensional incompressible flows', *University of Minnesota Supercomputer Institute Report UMSI 89/145*, 1989, to appear in *Computer Methods in Applied Mechanics and Engineering*.
5. T. E. Tezduyar, R. Glowinski and J. Liou, 'Petrov–Galerkin methods on multiply-connected domains for the vorticity–stream function formulation of the incompressible Navier–Stokes equations, *Int. j. numer. methods fluids*, **8**, 1269–1290 (1988).
6. M. S. Engelman and M. Jamnia, 'Transient flow past a circular cylinder', to appear in *Int. j. numer. methods fluids* (1990).